BIOCHEMISTRY
including biophysical chemistry & molecular biology

ARTICLE

pubs.acs.org/biochemistry

The Japanese Mutant Aβ (ΔE22-Aβ$_{1-39}$) Forms Fibrils Instantaneously, with Low-Thioflavin T Fluorescence: Seeding of Wild-Type Aβ$_{1-40}$ into Atypical Fibrils by ΔE22-Aβ$_{1-39}$

Adam L. Cloe,[‡] Joseph P. R. O. Orgel,[§] Joseph R. Sachleben,[†] Robert Tycko,[∥] and Stephen C. Meredith[*,‡,⊥]

[‡]Department of Pathology, The University of Chicago, Chicago, Illinois 60637, United States

[§]BioCAT and μCoSM, Pritzker Institute of Biomedical Science and Engineering, and CSRRI and Department of Biological Chemical and Physical Sciences, Illinois Institute of Technology, Chicago, Illinois 60616, United States

[∥]Laboratory of Chemical Physics, National Institute of Diabetes and Digestive and Kidney Diseases, National Institutes of Health, Bethesda, Maryland 20892-0520, United States

[⊥]Department of Biochemistry and Molecular Biology, The University of Chicago, Chicago, Illinois 60637, United States

[†]Biomolecular NMR Facility, Shared Research Facilities, The University of Chicago, Chicago, Illinois 60637, United States

Supporting Information

ABSTRACT: The ΔE693 (Japanese) mutation of the β-amyloid precursor protein leads to production of ΔE22-Aβ peptides such as ΔE22-Aβ$_{1-39}$. Despite reports that these peptides do not form fibrils, here we show that, on the contrary, the peptide forms fibrils essentially instantaneously. The fibrils are typical amyloid fibrils in all respects except that they cause only low levels of thioflavin T (ThT) fluorescence, which, however, develops with no lag phase. The fibrils bind ThT, but with a lower affinity and a smaller number of binding sites than wild-type (WT) Aβ$_{1-40}$. Fluorescence depolarization confirms extremely rapid aggregation of ΔE22-Aβ$_{1-39}$. Size exclusion chromatography (SEC) indicates very low concentrations of soluble monomer and oligomer, but only in the presence of some organic solvent, e.g., 2% (v/v) DMSO. The critical concentration is approximately 1 order of magnitude lower for ΔE22-Aβ$_{1-39}$ than for WT Aβ$_{1-40}$. Several lines of evidence point to an altered structure for ΔE22-Aβ$_{1-39}$ compared to that of WT Aβ$_{1-40}$ fibrils. In addition to differences in ThT binding and fluorescence, PITHIRDS-CT solid-state nuclear magnetic resonance (NMR) measurements of ΔE22-Aβ$_{1-39}$ are not compatible with the parallel in-register β-sheet generally observed for WT Aβ$_{1-40}$ fibrils. X-ray fibril diffraction showed different *D* spacings: 4.7 and 10.4 Å for WT Aβ$_{1-40}$ and 4.7 and 9.6 Å for ΔE22-Aβ$_{1-39}$. Equimolar mixtures of ΔE22-Aβ$_{1-39}$ and WT Aβ$_{1-40}$ also produced fibrils extremely rapidly, and by the criteria of ThT fluorescence and electron microscopic appearance, they were the same as fibrils made from pure ΔE22-Aβ$_{1-39}$. X-ray diffraction of fibrils formed from 1:1 molar mixtures of ΔE22-Aβ$_{1-39}$ and WT Aβ$_{1-40}$ showed the same *D* spacings as fibrils of the pure mutant peptide, not the wild-type peptide. These findings are consistent with extremely rapid nucleation by ΔE22-Aβ$_{1-39}$, followed by fibril extension by WT Aβ$_{1-40}$, and "conversion" of the wild-type peptide to a structure similar to that of the mutant peptide, in a manner reminiscent of the prion conversion phenomenon.

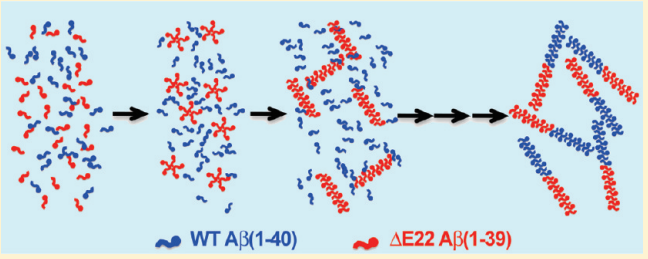

A small percentage of familial forms of Alzheimer's disease are caused by point mutations in the β-amyloid precursor protein (β-APP) within the sequence of the common forms of Aβ peptides. Of these, most occur at residues 21−23, including the Dutch (E22Q), Flemish (A21G), Italian (E22K), Arctic (E22G), and Iowa (D23N) mutants.[1−6] Wild-type (WT) Aβ$_{1-40}$ fibrils contain two parallel, in-register β-sheets, linked by an ordered, non-β-sheet bend region.[7−10] These mutations may fall near the boundary between the N-terminal β-sheet and the bend region. One might expect, therefore, that such mutations could have profound effects on either the aggregation kinetics, the structure of aggregates, or both.

Tomiyama et al. reported a new mutation in this part of β-APP, which gives rise to Aβ peptides missing E22, such as ΔE22-Aβ$_{1-39}$.[a] In marked contrast to both WT and most of the point mutant forms of Aβ mentioned above, however, ΔE22-Aβ peptides were reported not to form amyloid fibrils.[11] This conclusion was based primarily on three sets of findings: negative Pittsburgh B brain scan, absence of thioflavin T (ThT) fluorescence, and absence of fibrils in electron micrographs of synthetic ΔE22-Aβ. As the proband with this mutation is alive, it is not known whether neuritic plaques are present in the brain. These negative findings, however, go to the heart of a controversy in this field. Whereas the amyloid cascade hypothesis[12,13] holds that

Received: October 7, 2010
Revised: February 2, 2011
Published: February 03, 2011

formation of fibrils is a source of neuro- and cytotoxicity of protein aggregates, more recent studies have highlighted the importance of small, soluble oligomers of Aβ and other aggregating proteins.[14−16] The apparent inability of ΔE22-Aβ to form fibrils would lend support to the notion that fibrils are not the main neuro- and/or cytotoxins, and may even be innocuous or protective.[17]

Here, we show that contrary to previous reports, ΔE22-Aβ forms fibrils and does so "instantaneously", within the limits of several assays. These fibrils are typical amyloid, except for their apparently low level of thioflavin T binding and fluorescence. (As discussed below, these variables depend on which assay is used.) In addition, X-ray diffraction and preliminary solid-state NMR, among other data, suggest that the fibril structure differs from those of previously reported WT Aβ fibrils. Finally, we show below that when ΔE22-Aβ and WT Aβ are mixed in a disaggregating solvent and then transferred to buffer, the resulting fibrils are mutant-like, suggesting that the mutant peptide nucleates rapidly and templates the wild-type peptide, converting it to an alternate structure in a prion-like fashion.

MATERIALS AND METHODS

Peptide Synthesis and Purification. Peptides were synthesized on an Applied Biosystems (Foster City, CA) 433A synthesizer essentially as described previously.[18] Briefly, peptides were synthesized at a 0.25 mmol scale, using Fast-Moc chemistry with *N*-hydroxybenzotriazole (HOBT) and 2-(1*H*-benzotriazol-1-yl)-1,1,3,3-tetramethyluronium hexafluorophosphate (HBTU) (Peptides International) as coupling reagents and an Fmoc-Wang resin. Coupling times were extended by ∼3.3-fold; in addition, the following residues were doubly coupled: R5, S8, V11, V18, V24, G25, S26, and N27 (residue numbers refer to wild-type Aβ or the corresponding residues in ΔE22-Aβ_{1-39}). Peptides were cleaved from resin when the resin was stirred in 94% trifluoroacetic acid (TFA), 2.5% water, 2.5% ethanedithiol, and 1% triisopropylsilane (all v/v) in a closed flask for 2 h at room temperature and purified by reverse phase HPLC. Using these techniques, we synthesized and purified ΔE22-Aβ_{1-39} and WT Aβ_{1-40} using the standard techniques described above: NH_2-DAEFRHDSGY[10] EVHHQKLVFF[20] AEDVGSNKGA[30] IIG-LMVGGVV[40]-COOH and NH_2-DAEFRHDSGY[10] EVHHQ-KLVFF[20] ADVGSNKGAI[30] IGLMVGGVV[39]-COOH, respectively. Peptides were checked for purity by analytical reverse phase (C18) HPLC and MALDI-TOF mass spectrometry, as described previously.[20]

Electron Microscopy. Peptides were dissolved in neat DMSO and then diluted into sodium phosphate (pH 7.40) or Milli-Q purified water so that the final peptide concentration was 10 or 100 μM and the DMSO concentration was 2% (v/v). The solutions were allowed to aggregate at 37 °C. At various times (described in Results), aliquots of the fibril slurry were examined by electron microscopy by applying the slurry to glow-discharged, 400-mesh, carbon-coated support films. Because of matting of the ΔE22-Aβ_{1-39} fibrils, to obtain larger sample sizes for measuring mean diameters, we sonicated slurries for 30 min using a Branson ultrasonic cleaner and then examined them via electron microscopy as described. Measurements of ∼40 single ΔE22-Aβ_{1-39} fibrils suggested that sonication did not cause a change in mean fibril diameter; in addition, for WT Aβ_{1-40} fibrils, which do not form matted tangles as much as the mutant peptide, sonication did not alter mean fibril diameter. Samples were stained with 0.1% (w/v) uranyl acetate. Excess solution was wicked off with a paper tissue, and the grids were air-dried. Micrographs were imaged on an FEI Tecnai F30st-STEM microscope at magnifications of 15000×, 49000×, and 98000×. The CCD camera of the microscope added another 1.4× magnification to all images. Fibril diameters were measured using the freeware program Irfanview, with both freehand and straight-line selection tools. Fibril morphologies were compared against those of several other fibril preparations of different peptide stocks before final measurement of the dimensions.

Congo Red Binding. The Congo Red binding assay was performed essentially as described previously.[18] Briefly, an aliquot of peptide solution containing 50 μg of peptide was added to 1 mL of a 3 μM solution of Congo Red in 100 mM sodium phosphate (pH 7.40). The solution was incubated for 15 min at room temperature, and then the absorbance was measured from 400 to 600 nm.

Thioflavin T Fluorescence. We started fibrillization reactions by dissolving the lyophilized peptide, either WT-Aβ_{1-40} or ΔE22-Aβ_{1-39}, in neat DMSO so that the final DMSO concentration would be 2% (v/v). Peptide concentrations were typically 10 or 100 μM. Peptide concentrations were determined from the absorbance at 274.6 nm, using the extinction coefficient for tyrosine of 1420 M^{-1} cm^{-1}. Peptides were incubated at 37 °C in 10 mM sodium phosphate (pH 7.40) containing 0.01% (w/v) NaN_3. Fluorescence measurements were performed using a Hitachi F-2000 fluorescence spectrophotometer as described previously,[19−21] which is based on the assay described by LeVine.[22,23] In short, a 5 μL aliquot of slurry containing fibrils was added to 1 mL of a 10 μM thioflavin T solution in 10 mM sodium phosphate (pH 7.40). The solution was mixed vigorously by vortexing, and the fluorescence signal was then averaged for 10 s with the excitation and emission wavelengths set to 446 and 490 nm, respectively. The slit width was 1 mm.

Subsequently, we examined whether the apparently low ThT fluorescence of ΔE22-Aβ_{1-39} could be due, in part, to inaccessibility of the dye to binding sites on the tangled, matted fibril cords. To address this question, we performed ThT fluorescence assays by an alternate method,[24] in which 10 μM ThT was incorporated into the fibrillization reaction mixture. That is, fibrillization reactions were performed in stirred or unstirred fluorescence cuvettes and were initiated by dilution of Aβ peptides in neat DMSO into 10 mM sodium phosphate (pH 7.40) containing 10 μM ThT, so that the final DMSO concentration was 2% (v/v) and the peptide concentration 100 μM. The progress of the reaction was measured by periodically monitoring the fluorescence (same λ_{ex} and λ_{em} described above).

ThT Binding. Initial observations (see Results) indicated that ΔE22-Aβ_{1-39} forms fibrils, but with very low ThT fluorescence. To determine whether ΔE22-Aβ_{1-39} fibrils bind ThT, we developed an HPLC-based assay of ThT binding that does not rely on ThT fluorescence. For this assay, fibrils of wild-type Aβ_{1-40} and ΔE22-Aβ_{1-39} were formed by incubating 100 μM and 1 mM solutions of each peptide at 37 °C in 10 mM sodium phosphate (pH 7.40) with 0.01% NaN_3 (NaP), for ∼2 weeks, until mature fibrils had formed; 150 μL of 100 μM ThT [in 10 mM sodium phosphate (pH 7.40)] was added to various volumes of these peptide slurries and the volume adjusted with the same buffer to 1.5 mL. Thus, the final concentration of ThT was 10 μM. Various volumes of the fibril slurry were incubated in 10 mM ThT for 2 h at 37 °C, after which the samples were centrifuged for 2 h at 100000*g* using the Beckman Airfuge.

The top third of the supernatant was then removed, and the ThT concentration was assayed by injecting an aliquot with a known volume (generally 50 or 100 μL) onto a C18 reverse phase HPLC column. The sample was eluted using the following gradient: 5 min at 0% B, followed by a gradient from 100% A and 0% B to 55% A and 45% B over 55 min [where A is a 100:0.1 (v/v) water/TFA mixture and B is a 100:0.1 (v/v) methanol/TFA mixture]. The effluent was monitored at 430 nm. A sample chromatograph is shown in Figure 1A of the Supporting Information. The concentration of ThT was measured by integrating the peaks using Hewlett-Packard Chemstation to obtain the mass of ThT in the injected volume. A calibration curve (Figure 1B of the Supporting Information) was constructed by injecting various known volumes of a 10 mM solution of ThT. As shown in the figure, areas of the peaks were proportional to the mass of ThT in the injected sample.

For the purposes of comparing macroscopic binding of ThT to WT Aβ_{1-40} and ΔE22-Aβ_{1-39} fibrils, we analyzed data, using the simplest possible scheme, in which ThT in solution forms a complex with binding sites on the fibrils

$$T_f + S_f \rightleftharpoons Cx \quad (1)$$

where Cx is a complex between ThT and a binding site on the fibril, S_f denotes free sites on the fibril for ThT, and T_f is the free (unbound) ThT. Cx = T_b = bound ThT, and K_d is therefore

$$K_d = (S_f T_f)/Cx = S_f(10 - T_b)/T_b \quad (2)$$

In addition, $S_f = S_t - S_b = S_t - T_b$, where S_t is the total number of binding sites for ThT added and S_b is the number of sites on the fibril to which ThT is bound (occupied sites). Because the number of binding sites per peptide is not known a priori, we measured an apparent K_d ($K_d^{app} = nK_d$, where n is the number of sites per peptide). This yields the following quadratic equation:

$$K_d^{app} = (P_t - T_b)(10 - T_b)/T_b \quad (3)$$

from which K_d^{app} can be obtained. In addition, the number of sites per peptide can be estimated from the K_d^{app}, because at this concentration, $T_b = T_f = 5\ \mu$M and $n = K_d^{app}/5\ \mu$M. Although the binding of ThT to Aβ and other fibrils is complex and the binding sites are heterogeneous,[25−27] we use this phenomenological treatment solely to compare WT and mutant Aβ fibrils.

Critical Concentration (C_r) of WT Aβ_{1-40} and ΔE22-Aβ_{1-39}. For amyloid-forming peptides, a critical concentration (C_r) can be defined as the concentration of peptide remaining in solution at equilibrium, which can be approached by either formation of fibril at infinite time or dissolution of preformed fibrils, also at infinite time.[28] In practice, this parameter is estimated by extrapolation to infinite time from the fit of rate equations to experimental data; i.e., $P = (P_0 - P_{eq}) \times \exp(-kt) + P_{eq}$, where P is the soluble peptide concentration, P_0 is the initial soluble peptide concentration, P_{eq} is the soluble peptide concentration at equilibrium, k is the apparent first-order rate constant, and t is the time.

Initial observations suggested that C_r for ΔE22-Aβ_{1-39} might be at or below the limits of detection of many commonly used protein assays, such as the microBCA assay (limit of detection of ~0.5 μg/mL = 0.12 μM ΔE22-Aβ_{1-39}). This was subsequently confirmed. For this reason, we analyzed protein concentrations by first hydrolyzing the peptide to "amplify the signal" of protein and then using a sensitive fluorescence assay, i.e., fluorescamine assay. Peptides were hydrolyzed for 16 h at 100 °C in 0.2 mL of 6 M HCl. The solution was lyophilized, after which the powder was dissolved in 1 mL of 0.2 M sodium borate (pH 9.00) for the fluorescamine assay. Fluorescamine was freshly dissolved to a final concentration of 0.1 mg/mL in acetone; 0.15 mL of this solution was added to the hydrolyzed protein solution. After the solution had been vortexed, fluorescence was measured with a λ_{ex} of 390 nm and a λ_{em} of 475 nm.

The mass of the protein present in the sample was calculated from a calibration curve constructed from aliquots of authentic WT Aβ_{1-40} and ΔE22-Aβ_{1-39} [masses of peptide between 0 and 0.625 μg of peptide (from 0 to 250 μL of peptide stock solutions at 2.5 μg/mL) that had undergone the same hydrolysis and subsequent treatment, as described above]. Figure 2 of the Supporting Information shows the calibration curves for WT Aβ_{1-40} (○) and ΔE22-Aβ_{1-39} (●), which are essentially superimposable. In both cases, the curves were nonlinear and could be fit to the equation of a straight line plus a hyperbola: for WT Aβ_{1-40}, $F = 95.14 + 1.44 \times 10^{12} \times M + 229.2 \times M/(8.10 \times 10^{-12} \times M)$, where F is the fluorescence and M is the number of moles of peptide.

Size Exclusion Chromatography. Wild-type Aβ_{1-40} and ΔE22-Aβ_{1-39} were freshly disaggregated by dissolving them in neat DMSO for ~1 h immediately prior to chromatography. Solutions were centrifuged at 14300*g* for 20 min, before samples were injected onto the column. Peptides were injected onto the column either in neat DMSO at a peptide concentration of 100 μM or after being diluted to a final concentration of 10 or 100 μM with 10 mM sodium phosphate (pH 7.40) [with 0.1% (v/v) NaN_3]. The column was a Superdex Peptide 10/300 column (GE Healthcare). The eluant was 10 mM sodium phosphate (pH 7.4) containing 2% (v/v) DMSO. When the same buffer without DMSO was used as the eluant, none of the ΔE22-Aβ_{1-39} emerged from the column, presumably because it precipitated onto the column matrix. Chromatography was performed using an Agilent model 1100 HPLC system. The flow rate was 0.45 or 0.5 mL/min. The temperature was ~22 °C, and the effluent was monitored at 220, 230, and 274 nm. Apparent molecular weights (MW^{app}) were estimated from a calibration curve constructed using the following standards: horse myoglobin (16951.5), cytochrome *c* (12372), E7-peptide dimer (8431), aprotinin (6512), E7-peptide (4215.5), vitamin B_{12} (1350), and glycine (75) (molecular weights in parentheses). E7-peptide is a synthetic peptide from the E7 protein of human papillomavirus type 16. We synthesized it using standard "Fast-Moc" FMOC chemistry, as described above, for purposes other than the studies in this paper; the molecular weight of the monomer was determined by MALDI-TOF mass spectrometry. The calibration curve using these peptides is contained in the Supporting Information of ref 29.

X-ray Diffraction. X-ray diffraction data were obtained for fibrils of WT Aβ_{1-40} and ΔE22-Aβ_{1-39}, essentially as described previously.[21] Briefly, fibrils formed as described above were washed by dialysis against distilled water, centrifuged, and placed into 0.7 mm glass capillaries (Charles Supper). Prior to obtaining X-ray diffraction data, the capillary tubes containing fibrils were placed onto the surface of a 11.7 T NMR magnet for 5 days, which achieved partial alignment of fibrils (see also refs 30 and 31). Synchrotron data were collected at Argonne National Laboratory, Advanced Photon Source beamline BioCAT, on a CCD-based X-ray detector (PCCD 168080/Aviex LLC). Other conditions and methods of analysis were as described previously.[19]

Circular Dichroism Spectroscopy. Circular dichroism (CD) spectra were recorded using an Aviv (Lakewood, NJ) model 202 spectropolarimeter with a temperature-controlled cuvette holder. Samples were disaggregated in 20 μL of neat hexafluoro-2-propanol (HFIP) and then diluted to a concentration 100 μM in 10 mM phosphate buffer (pH 7.4). Diluted samples were added to a 0.1 cm path length cell (Starna), and five scans were obtained from 280 to 180 nm at intervals of 1 nm with a 1 s averaging time. The temperature of the cuvette holder was 25 °C. The bandwidth was 1 nm. Data were collected in the form of sample dynode and sample raw ellipticity signal. Buffer signals were subtracted from each scan, and all scans were zeroed by subtracting the mean of ellipticity values between 255 and 260 nm for all scans of each peptide.

Fluorescence Depolarization. To obtain a measure of peptide aggregation that is independent of thioflavin T binding or fluorescence, we measured fluorescence anisotropy as a function of time. To begin the experiment, we added a solution containing 0.04 or 0.4 mg of either WT-Aβ_{1-40} or ΔE22-Aβ_{1-39} in 20 μL of neat DMSO to 980 μL of 0.01 M sodium phosphate (pH 7.40) and 0.01% (w/v) NaN_3. Final peptide concentrations were either 10 or 100 μM. The solutions were gently inverted to mix the solution, and fluorescence spectra were recorded immediately thereafter, with a delay of $\leq$1 min. In some experiments, we made mixtures of WT Aβ_{1-40} and ΔE22-Aβ_{1-39} by mixing peptides in DMSO prior to adding the peptides to aqueous buffers, generally 0.01 M sodium phosphate (pH 7.40) containing 0.01% (w/v) NaN_3. In these experiments, as in the previous experiments, the final concentration of DMSO was 2% (v/v) and the final total peptide concentration was either 10 or 100 μM.

The samples were excited at 275 nm, for the single intrinsic Tyr fluor in either peptide (both peptides have one Tyr residue and no Trp residues). The samples were excited first with the presample polarizer in the vertical (0°) position; emission spectra were then recorded, with the postsample polarizer first in the vertical (0°) and then the horizontal (90°) position. Next, samples were excited with the presample polarizer in the horizontal (90°) position; emission spectra were then recorded, with the postsample polarizer first in the vertical (0°) and then the horizontal (90°) position. Anisotropy (A) is defined as follows:

$$A = \frac{I_{VV} - GI_{VH}}{I_{VV} + 2GI_{VH}}$$

where G is an instrument correction factor that compensates for any polarization bias of the detection system.[32] G is defined as

$$G = I_{HV}/I_{HH}$$

Spectra were recorded at intervals of 5 min from 0 to 60 min. Measurements of anisotropy were taken at the peak of the emission spectrum, ~307 nm; fluorescence values at 307 nm were smoothed by interpolating the values from 300 to 315 nm.

Solid-State NMR. Peptides containing single ^{13}C labels were synthesized for solid-state NMR studies as follows: ΔE22-Aβ_{1-39} containing 1-^{13}C-V36, ΔE22-Aβ_{1-39} containing 1-^{13}C-V18, and WT-Aβ_{1-40} containing 1-^{13}C-V12. Peptides were synthesized and purified as described above. Fibril slurries were made as described above; salts were removed by dialysis against Milli-Q water, using dialysis tubing with a molecular weight cutoff of 500, followed by three cycles of centrifugation of water at 14300g for 30 min in siliconized Eppendorf tubes and resuspension of the fibrils in Milli-Q water. The final pellet was flash-frozen and lyophilized, and the lyophilized samples (approximately 5 mg each) were packed into 3.2 mm magic angle spinning (MAS) rotors with Teflon spacers to contain the samples in the center of the NMR solenoid coil. Solid-state NMR measurements were taken at 9.4 T (100.4 MHz ^{13}C NMR frequency), using three-channel 3.2 mm MAS probes (Varian) and Varian InfinityPlus spectrometer consoles. To assess distances between ^{13}C labels in adjacent peptide molecules, we performed homonuclear dipolar recoupling experiments using the PITHIRDS-CT recoupling technique.[33] Measurements of $^{13}C-^{13}C$ dipole−dipole couplings were performed at 9.4 T and a 20.00 kHz MAS frequency. Radiofrquency (Rf) pulses were actively synchronized with an MAS tachometer signal.

Analytical Reverse Phase HPLC Separation of Soluble ΔE22-Aβ_{1-39} and WT Aβ_{1-40} from Cofibrillizing Mixtures. Experiments in which a 1:1 (molar) mixture of ΔE22-Aβ_{1-39} and WT Aβ_{1-40} in neat DMSO is transferred into aqueous buffer [10 mM sodium phosphate (pH 7.40) with 0.01% NaN_3 (NaP)] for fibrillization of the mixture will be presented below. We developed an analytical reverse phase HPLC assay to determine the concentration of each peptide remaining in solution at various times; 100 μL aliquots of the mixed fibril slurries were centrifuged using a Beckman Airfuge at 100000g for 1 h. The top 30 μL of the supernatant was injected onto a Zorbax C18 analytical HPLC column and chromatographed isocratically using a 68:32 (v/v) A/B mixture, where A is 0.1% (v/v) TFA in water and B is 0.1% (v/v) TFA in acetonitrile. The column was heated to 60 °C. The column effluent was monitored by absorbance at 210 nm. A calibration curve was constructed from aliquots from stock solutions, to contain known masses of each peptide (concentrations determined by UV spectroscopy, as described above). Figure 3A of the Supporting Information shows a typical chromatographic separation of ΔE22-Aβ_{1-39} and WT Aβ_{1-40}, using this isocratic solvent system. The two peptides elute as clearly separated peaks, which were integrated using Hewlett-Packard Chemstation to obtain the mass of each peptide.

Experimental data were analyzed by a nonlinear least-squares fit to the equation of a first-order approach to equilibrium, $P = P_{eq} + (P_0 - P_{eq}) \times \exp(-kt)$, where P is the peptide concentration at various times, P_0 is the initial peptide concentration (50 μM), and P_{eq} is the peptide concentration at equilibrium. Because the centrifugation step took 1 h, this was added to the time for kinetic analysis.

$^1H-^{15}N$ HSQC NMR spectra of ΔE22-Aβ_{1-39} and WT Aβ_{1-40}. The rapid fibrillization by ΔE22-Aβ_{1-39} raised the question of whether this peptide had been fully disaggregated by being dissolved in DMSO. We addressed the question of whether the peptide is fully disaggregated, within experimental limits of detection, by obtaining $^1H-^{15}N$ HSQC NMR spectra of ΔE22-Aβ_{1-39} dissolved in DMSO-d_6. Natural abundance $^1H-^{15}N$ HSQC spectra[34] were recorded on a Varian Unity Inova NMR spectrometer equipped with a cryogenically cooled "Cold Probe", operating at a ^1H frequency of 601 MHz and a ^{15}N frequency of 61 MHz. The HSQC experiment was conducted with the standard Varian pulse sequence gNhsqc; 128 transients with 4096 complex points were signal-averaged over a proton sweep width of 9615.4 Hz in the direct dimension. The acquisition time in the direct dimension was 0.43 s; 128 complex points were taken in the indirect (^{15}N) dimension over a sweep width

of 1944 Hz, giving an acquisition time of 0.066 s. Quadrature detection in the indirect dimension was achieved via the echo−antiecho method. With a recycle delay of 1 s, the total experiment time was approximately 9 h.

RESULTS

ΔE22-Aβ_{1-39} Forms Fibrils Very Rapidly, but with Low Thioflavin T Fluorescence. We assayed fibrillization of ΔE22-Aβ_{1-39} and WT Aβ_{1-40} by ThT fluorescence (Figure 1). Peptides were first dissolved in neat DMSO and then diluted to the appropriate concentrations, typically 100 μM, using NaP, so that the final DMSO concentration was 2% (v/v). Attempts to dissolve ΔE22-Aβ_{1-39} directly in aqueous media without DMSO or other organic solvents did not produce measurable quantities of peptide in solution. After peptides had been dissolved in DMSO and transferred to buffer, they were incubated at 37 °C under quiescent conditions. Although ΔE22-Aβ_{1-39} induced little ThT fluorescence, in agreement with previous reports,[11] a small amount of ThT fluorescence above the background appeared "instantaneously" and remained essentially constant during a 2 week incubation. This contrasts with the well-known pattern for unseeded WT Aβ_{1-40} fibrillization (Figure 1), in which ThT fluorescence rises rapidly only after a lag period of ∼2−3 days. The latter kinetic pattern has been attributed to a nucleation−polymerization mechanism of fibril formation.[35−37]

Immediately upon transfer of a solution of ΔE22-Aβ_{1-39} in neat DMSO into NaP, a visible precipitate appeared. This slurry was examined by electron microscopy; the slurry was also examined after incubation for 7 days at 37 °C. In the case of WT Aβ_{1-40}, formation of a precipitate required incubation for several days at 37 °C, which is consistent with the ThT fluorescence data. Electron microscopy of the ΔE22-Aβ_{1-39} precipitates revealed numerous, abundant fibrils, both immediately after introduction of the peptide into buffer (Figure 2A−C) and after incubation for 7 days at 37 °C (Figure 2D−F); the appearance of the fibrils did not change upon incubation. The ΔE22-Aβ_{1-39} fibrils have a slightly irregular edge. Only occasional fibrils show an apparent "twist"; more fibrils appear as flat ribbons with longitudinal striations. Fibrils of ΔE22-Aβ_{1-39} had a strong tendency to supertwist into matted, thick, ropelike helical bundles. Diameters of WT Aβ_{1-40} and ΔE22-Aβ_{1-39} fibrils were measured (Figure 2I). ΔE22-Aβ_{1-39} fibrils had a slightly smaller mean diameter (9.44 ± 2.56 nm) than WT Aβ_{1-40} fibrils (11.0 ± 2.44 nm).

One method of obtaining single, unmatted ΔE22-Aβ_{1-39} fibrils for measuring diameters was to form the fibrils at low peptide concentrations. As shown in Figure 4 of the Supporting Information, fibrils were present even when the initial concentration was a low as 1 μM.

^{1}H−^{15}N HSQC NMR Spectra of ΔE22-Aβ_{1-39} and WT Aβ_{1-40}. The very rapid formation of ΔE22-Aβ_{1-39} fibrils raises the question of whether DMSO completely disaggregates the lyophilized peptide. To address this question, we obtained ^{1}H−^{15}N HSQC spectra of ΔE22-Aβ_{1-39} in DMSO-d_6, reasoning that if monomers and an aggregated soluble species were both present in DMSO, there would be more than one peak per amide for some of the amides in the peptide. As shown in Figure 5 of the Supporting Information, the spectrum of ΔE22-Aβ_{1-39} contains 39 peaks, consistent with 37 of the 38 backbone amides in the peptide, plus the two amide side chains for the one Asn and one Gln in the peptide. WT Aβ_{1-40} gave a similar ^{1}H−^{15}N HSQC spectrum, containing 40 peaks, again consistent with one peak per amide. These results suggest that only a single species of each peptide exists in solution, either a monomer or, if oligomeric, a single species in which all molecules are in a symmetrical arrangement. By this criterion, ΔE22-Aβ_{1-39} is as fully disaggregated by DMSO as WT Aβ_{1-40}.

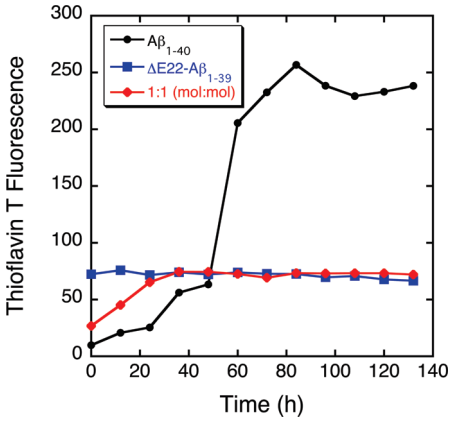

Figure 1. Thioflavin T fluorescence time course. Peptides were dissolved in neat DMSO and then diluted into aqueous buffer (NaP) so that the final peptide concentration was 100 μM and the DMSO concentration was 2% (v/v). At various intervals, aliquots were removed from the slurry, and thioflavin T fluorescence was measured as described in Materials and Methods. For the mixtures, peptides were dissolved and mixed in neat DMSO so that the final total peptide concentration was 100 μM and the DMSO concentration was 2% (v/v): (circles) WT Aβ_{1-40}, (squares) ΔE22-Aβ_{1-39}, and (diamonds) 1:1 (molar) mixture of WT Aβ_{1-40} and ΔE22-Aβ_{1-39}.

Binding of ThT to Fibrils, Access of ThT to Binding Sites, and Congo Red Binding to Fibrils. The low, easily overlooked level of ThT fluorescence could be due to a structural difference between WT Aβ_{1-40} and ΔE22-Aβ_{1-39} fibrils. (Other possibilities are considered below.) We next determined whether the relative lack of ThT fluorescence induced by ΔE22-Aβ_{1-39} fibrils was due to lack of ThT binding, a lack of fluorescence of bound ThT, or both. Accordingly, we developed an HPLC-based assay for ThT binding that was independent of fluorescence (see Materials and Methods). The results of these experiments (Figure 3A, for WT Aβ_{1-40} and ΔE22-Aβ_{1-39} fibrils) indicate that both the apparent K_d and the number of binding sites for ThT are reduced for ΔE22-Aβ_{1-39} fibrils compared to those for WT Aβ_{1-40} fibrils. The K_d values for WT Aβ_{1-40} and ΔE22-Aβ_{1-39} were 0.54 and 2.39 mM, respectively. The number of binding sites for ThT is far fewer than the number of peptide molecules, 510.5 and 117.0 for WT Aβ_{1-40} and ΔE22-Aβ_{1-39}, respectively. The binding sites for ThT on Aβ fibrils are heterogeneous;[25−27] the equation is a phenomenological binding isotherm, used only to compare slurries of WT and mutant Aβ fibrils.

An additional potential cause of the reduction in the number and affinity of binding sites for ThT in ΔE22-Aβ_{1-39} fibrils is the matting of the fibrils, which could prevent access of ThT to binding sites on fibrils. This could cause an underestimate of the number of binding sites. By the commonly employed ThT fluorescence assays used in the experiments described above, aliquots of a fibril slurry are added to a solution of ThT for fluorescence measurements. Because ΔE22-Aβ_{1-39} forms fibrils very rapidly and by electron microscopy the fibrils are matted

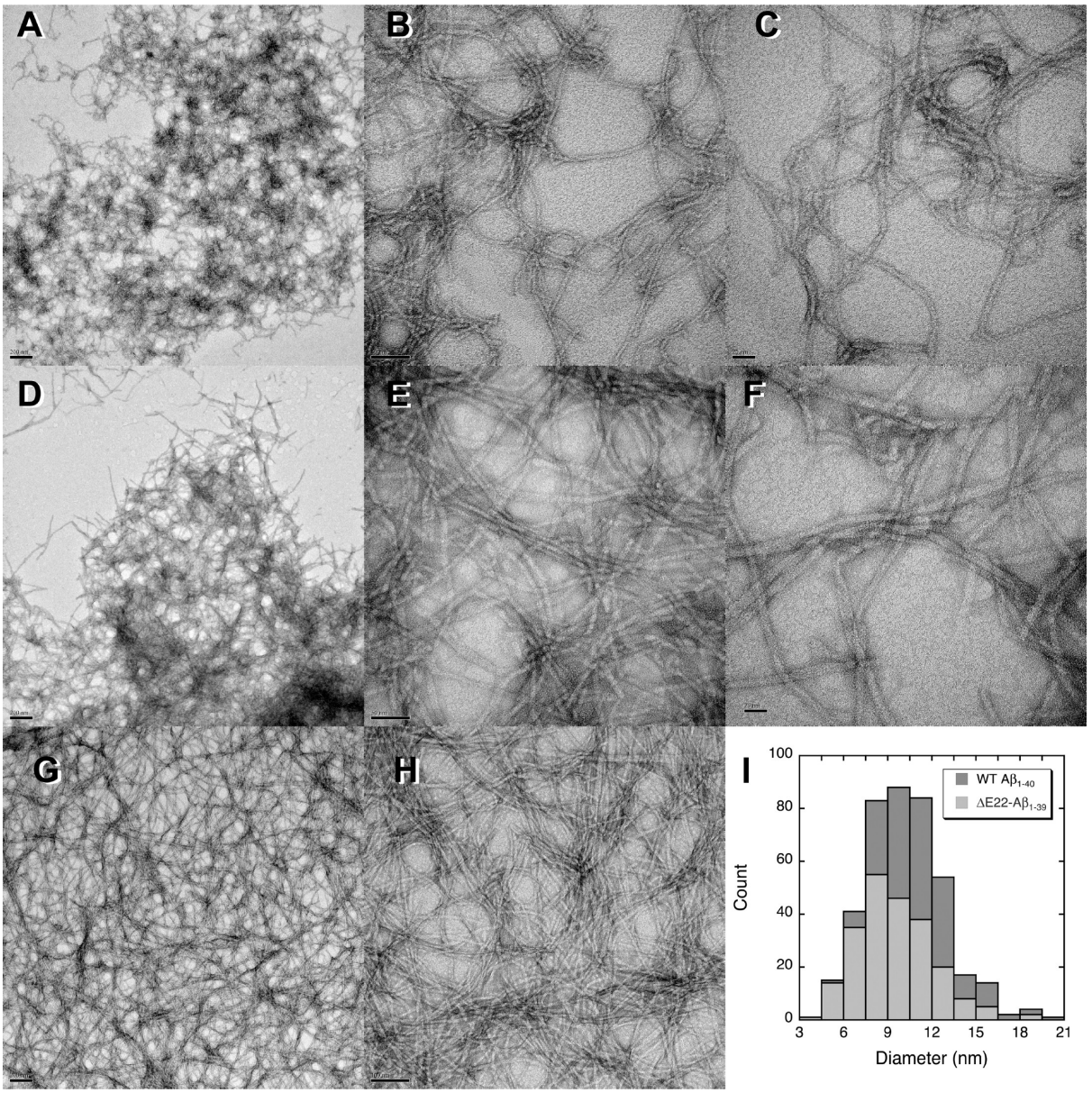

Figure 2. Electron micrographs of ΔE22-Aβ_{1-39} fibrils. Peptide was dissolved in DMSO and then diluted into NaP so that the peptide concentration was 100 μM and the final concentration of DMSO was 2% (v/v). A precipitate appeared instantly. Panels A−C show peptide immediately after addition of NaP to the peptide in neat DMSO. Magnifications are 15000×, 98000×, and 149000×. The images in panels A−C were taken immediately after the peptide had been transferred from neat DMSO to buffer and were viewed within 5 min of making the sample. Panels D−F are images of the same slurry after incubation for 7 days at 37 °C. Panels G and H are electron micrographs of fibrils of a 1:1 (molar) mixture of WT Aβ_{1-40} and ΔE22-Aβ_{1-39}. Peptides were dissolved in neat DMSO and then diluted with NaP so that the final concentration of each peptide was 50 μM (i.e., total peptide concentration of 100 μM) and the final DMSO concentration was 2%. A precipitate formed immediately. Magnifications of 15000× and 49000× for panels G and H, respectively. For all images, the CCD camera added a magnification of 1.4×. (I) Histograms for ΔE22-Aβ_{1-39} and WT Aβ_{1-40} fibril diameters, based on 200 and 400 diameter measurements, respectively. For both peptides, the histograms showed a single peak; means ± standard deviations were 11.0 ± 2.44 nm for WT Aβ_{1-40} fibrils and 9.44 ± 2.56 nm for ΔE22-Aβ_{1-39} fibrils.

even at the earliest time points, we sought to determine whether the low level of ThT binding by ΔE22-Aβ_{1-39} fibrils could be due to the inability of ThT to penetrate fibril bundles to reach binding sites. Accordingly, we performed ThT fluorescence assays in which the dye was included in the solution of the fibrillizing peptide. As shown in Figure 6 of the Supporting Information, the development of ThT fluorescence was essentially instantaneous. The fluorescence intensity was now somewhat higher, which can be attributed to the greater fibril:ThT ratio. WT Aβ_{1-40} developed fibrils that gave high ThT fluorescence after 2−3 days. Again, the fluorescence intensity of WT Aβ_{1-40} fibrils was much higher than that of ΔE22-Aβ_{1-39} fibrils. The difference between WT and mutant fibrils was somewhat smaller than when ThT fluorescence was assayed from aliquots, as in Figure 1. Thus, a small part of the low ThT fluorescence of mutant fibrils is caused by the lack of access of the dye to potential binding sites. Nevertheless, an intrinsic difference remains between the two types of fibrils, by either assay.

dx.doi.org/10.1021/bi1016217 |*Biochemistry* 2011, 50, 2026–2039

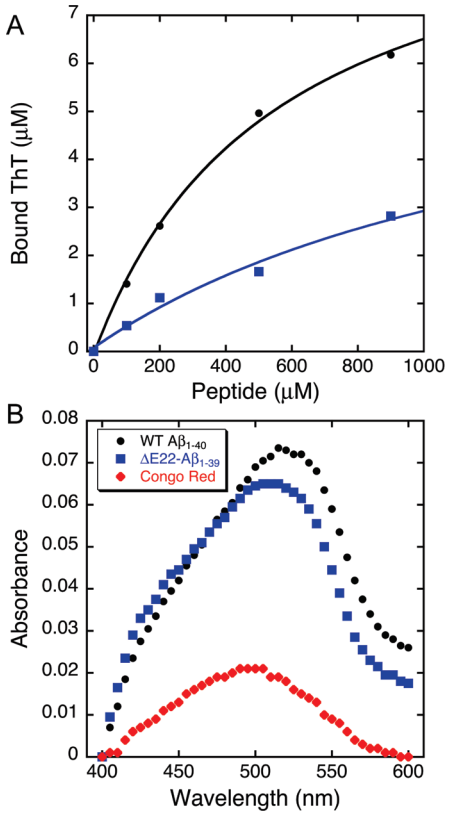

Figure 3. (A) Binding of ThT to WT Aβ_{1-40} (circles) and ΔE22-Aβ_{1-39} (squares) fibrils. Various volumes of fibril slurries (nominal peptide concentration of 1 mM) were added to a solution of ThT, as described in Materials and Methods. After an incubation period, the mixture was centrifuged and the supernatant analyzed for ThT concentration by HPLC. (B) Congo Red absorbance in the presence of WT Aβ_{1-40} (circles) and ΔE22-Aβ_{1-39} (squares) fibrils; the figure also shows the spectrum of Congo Red alone (diamonds).

We also tested whether ΔE22-Aβ_{1-39} fibrils cause the same shift in the visible spectrum of Congo Red (CR) as WT Aβ_{1-40} fibrils. WT and mutant fibrils caused similar spectral shifts in CR (Figure 3B). The absorbance maxima are ~517 and ~508 nm for WT Aβ_{1-40} and ΔE22-Aβ_{1-39}, respectively. The fact that both mutant and WT Aβ fibrils bind CR similarly, but not ThT, suggests that the binding sites for these two dyes do not entirely overlap.

Critical Concentrations of WT Aβ_{1-40} and ΔE22-Aβ_{1-39}. In this set of experiments, critical concentrations (C_r) were estimated for WT Aβ_{1-40} and ΔE22-Aβ_{1-39} by incubation of 100 μM solutions of each peptide for 3 weeks and subsequent seeding every 2.5 days with 5 μL of a slurry of mature fibrils. The slurries were then allowed to incubate under quiescent conditions for ≥2 weeks. As described in Materials and Methods, the peptide remaining in solution was assayed by centrifugation of the slurry twice at 100000*g*, after which the peptide remaining in solution was assayed by hydrolyzing the peptide and measuring the fluorescamine-associated fluorescence. As shown in Figure 4, the fluorescamine fluorescence reached final value of 496 and 223, corresponding to C_r values of 2.89 and 0.167 μM for WT Aβ_{1-40} and ΔE22-Aβ_{1-39}, respectively. Because our value for the C_r of WT Aβ_{1-40} was somewhat higher than that previously reported,[28] we considered the possibility that some of the peptide had been oxidized or hydrolyzed during the prolonged incubation. We centrifuged the slurry at 100000*g* using the Airfuge, isolated the supernatant, and analyzed this peptide by HPLC and MALDI-TOF mass spectrometry. HPLC showed the peptide to coelute with authentic WT Aβ_{1-40}, and mass spectrometry revealed the usual mass for the intact peptide, without evidence of oxidation. We conclude that this small difference may be due to minor differences between our solubilization or assay procedures and those used in other laboratories.

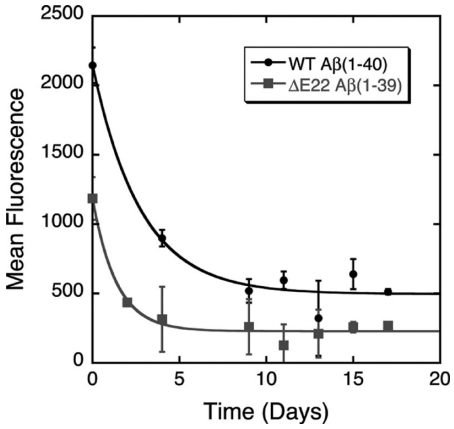

Figure 4. Critical concentrations of WT Aβ_{1-40} (●) and ΔE22-Aβ_{1-39} (■) estimated by seeding solutions of these peptides with fibrillar seeds, as described in Materials and Methods. At various times, aliquots were removed to determine the concentration of peptide in solution, using the fluorescamine assay described in Materials and Methods. The critical concentration was estimated from a fit of the data to the equation of a first-order approach to equilibrium.

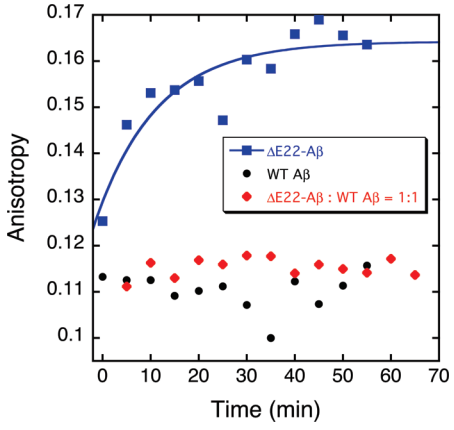

Figure 5. Fluorescence depolarization for (circles) WT Aβ_{1-40}, (squares) ΔE22-Aβ_{1-39}, and (diamonds) a 1:1 (molar) mixture of WT Aβ_{1-40} and ΔE22-Aβ_{1-39}. The line represents a nonlinear least-squares fit of the data to the first-order rate equation $A = (A_\infty - A_0)[1 - \exp(-kt)] + A_0$, where A, A_0, and A_∞ are the anisotropies at time t, time zero, and infinite time, respectively, and k is the rate constant.

Fluorescence Depolarization Experiments Show Very Rapid Aggregation of ΔE22-Aβ_{1-39}. We performed fluorescence depolarization to examine the early stages of aggregation of ΔE22-Aβ_{1-39} by a method that is independent of ThT fluorescence. As described in Materials and Methods, solutions of ΔE22-Aβ_{1-39} and WT Aβ_{1-40} were excited at a λ_{ex} of 275 nm, and emission spectra were recorded at 5 min intervals from 290 to 350 nm. Both peptides contain a single Tyr residue and no Trp residues.

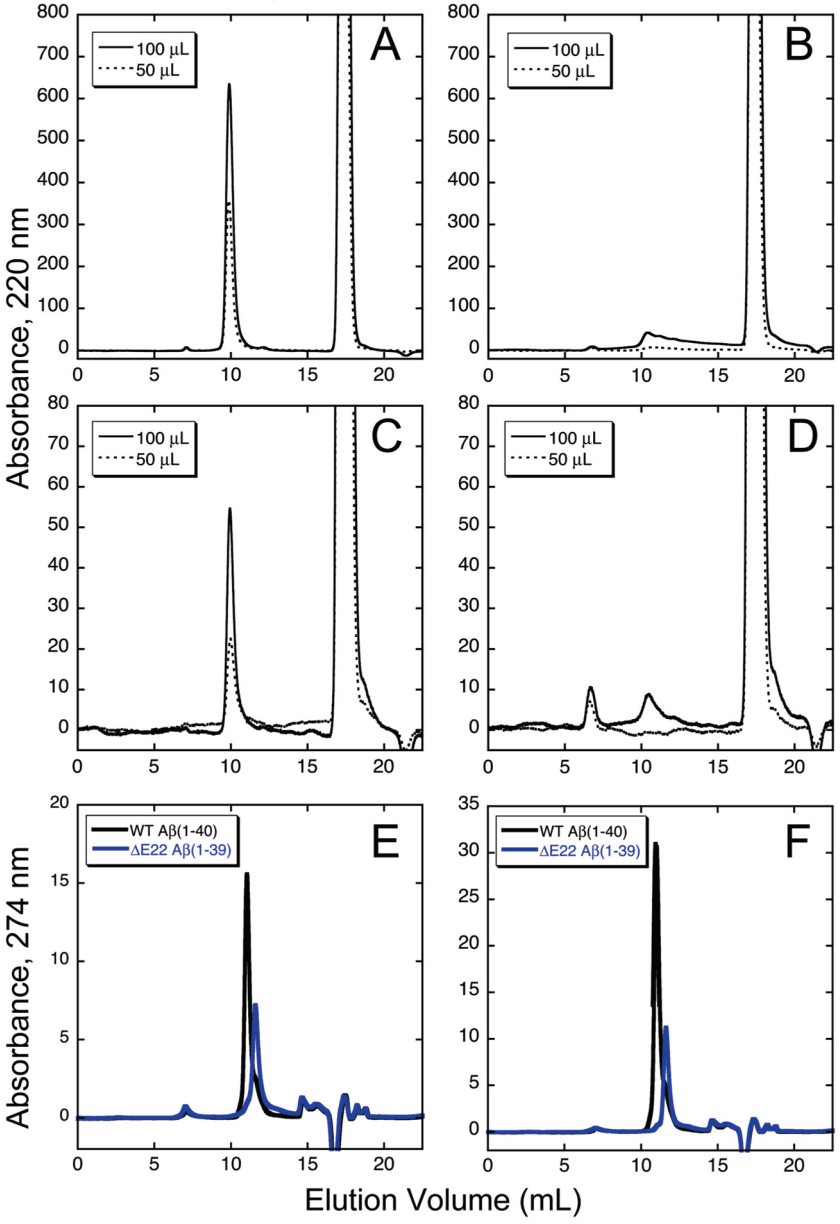

Figure 6. Size exclusion chromatography of WT Aβ_{1-40} and ΔE22-Aβ_{1-39} performed using a Superdex Peptide 10/300 column. For panels A−D, the peptide was initially dissolved in neat DMSO, which was diluted with NaP so that the final peptide concentration was 100 (A and B) or 10 μM (C and D). The eluant was NaP, without DMSO. For panels E and F, the peptide concentrations were 100 and 200 μM, respectively, and the samples were prepared as described for panels A−D. The eluant, however, was NaP containing 2% (v/v) DMSO: (A) 100 μM WT Aβ_{1-40}, (B) 100 μM ΔE22-Aβ_{1-39}, (C) 10 μM WT Aβ_{1-40}, (D) 100 μM ΔE22-Aβ_{1-39}, (E) 100 μM WT Aβ_{1-40} (black) or ΔE22-Aβ_{1-39} (blue), and (F) 200 μM WT Aβ_{1-40} (black) or ΔE22-Aβ_{1-39} (blue). For panels A−D, the effluent was monitored at 220 nm; for panels E and F, the effluent was monitored at 274 nm rather than 220 nm, because of the presence of DMSO in the eluant.

Measurements of both peptides were taken at 10 and 100 μM. The anisotropy of ΔE22-Aβ_{1-39} at 100 μM could not be measured because the peptide precipitated too rapidly from solution (all fluorescence intensities decreased *pari passu*, and the signal was essentially absent after ~5 min). Figure 5 shows the fluorescence anisotropy of WT Aβ_{1-40} at 100 μM and ΔE22-Aβ_{1-39} at 10 μM at times up to 60 min (a similar profile is seen for WT Aβ_{1-40} at 10 μM). The anisotropy of WT Aβ_{1-40} remains constant over the course of the experiment, indicating that no change occurs in the state of aggregation of this peptide. In contrast, ΔE22-Aβ_{1-39} undergoes a rapid increase in anisotropy, even at 10 μM, indicating aggregation of the peptide within this time period. The increase in anisotropy could be fit as a first-order rate equation, with a k of 0.08 s^{-1}.

Size Exclusion Chromatography (SEC) Shows That ΔE22-Aβ_{1-39} Forms Oligomers but Requires Organic Solvent (DMSO) To Elute from the Column. The preceding experiments indicate that ΔE22-Aβ_{1-39} can form fibrils instantaneously, within the limits of the techniques described above, with no evident lag phase in the kinetics. Size exclusion chromatography (Superdex Peptide column) gives an indication of the completeness of fibrillization of ΔE22-Aβ_{1-39}. Attempts to

dx.doi.org/10.1021/bi1016217 |*Biochemistry* 2011, 50, 2026–2039

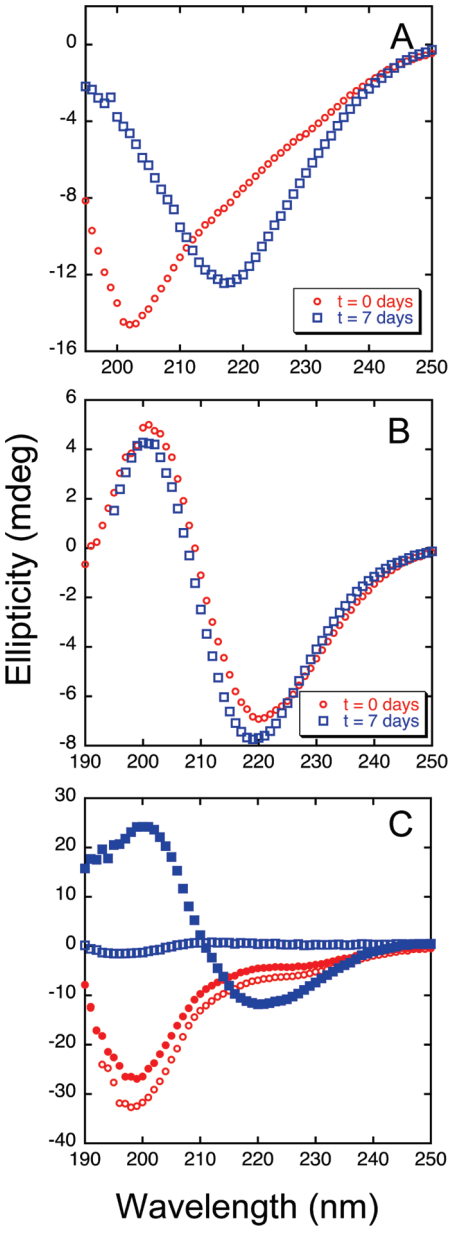

Figure 7. CD spectra of WT Aβ_{1-40} and ΔE22-Aβ_{1-39}. (A) WT Aβ_{1-40} was dissolved in HFIP and then diluted to a final peptide concentration of 100 μM with NaP. Spectra were recorded immediately after dilution of the peptide into NaP (t = 0 days, red) and after incubation at 37 °C for 7 days (t = 7 days, blue). (B) ΔE22-Aβ_{1-39}, treated the same as WT Aβ_{1-40} in panel A. (C) WT Aβ_{1-40} (red) and ΔE22-Aβ_{1-39} (blue) were dissolved in HFIP and then diluted with NaP as described for panels A and B. Immediately after the sample had been diluted into NaP, an initial CD spectrum was measured and the mixture was then centrifuged at 14300g, and the CD spectra of the supernatants (top 1 mL out of 1.5 mL in the centrifuge tube) were measured: (filled circles) WT Aβ_{1-40} before centrifugation, (empty circles) WT Aβ_{1-40} supernatant, (filled squares) ΔE22-Aβ_{1-39} before centrifugation, and (empty squares) ΔE22-Aβ_{1-39} supernatant.

dissolve ΔE22-Aβ_{1-39} in aqueous buffer and then perform SEC never resulted in elution of peptide from the column. When ΔE22-Aβ_{1-39} was first dissolved in neat DMSO and then diluted with NaP to a final concentration of 100 μM [2% (v/v) DMSO], only a miniscule peak eluted from the column, approximately in the same position as WT Aβ_{1-40} when the eluant was NaP (Figure 6A,B). The same experiment was attempted using only 10 μM peptide (panels C and D of Figure 6 for WT Aβ_{1-40} and ΔE22-Aβ_{1-39}, respectively). Panels E and F of Figure 6 show elution profiles when the same experiment was repeated, except that the eluant also contained 2% (v/v) DMSO. Elution of anything more than a trace of ΔE22-Aβ_{1-39} from the column appeared to require the presence of an organic solvent such as DMSO.

WT Aβ_{1-40} (Figure 6A,C) elutes predominantly as a peak (~10 mL) with an apparent molecular weight (5528) consistent with a monomer or dimer. The limited resolution of the column does not allow discrimination between these species. A second peak with a smaller area elutes near the void volume (~8 mL), presumably as oligomers of the peptide. ΔE22-Aβ_{1-39} consistently eluted at a slightly later time (lower apparent molecular weight of 4606) than the WT peptide (Figure 6E,F). In addition, although the same quantities of WT Aβ_{1-40} and ΔE22-Aβ_{1-39} were loaded onto the column, less mutant peptide eluted from it, suggesting that some of this peptide had precipitated on the column.

CD Spectroscopy Indicates that ΔE22-Aβ_{1-39} Adopts a β-Sheet Conformation "Instantly". ΔE22-Aβ_{1-39} could not be dissolved into NaP from a lyophilized powder, and thus, its CD spectra could not be obtained without adding organic solvent, e.g., HFIP. Figure 7B shows the CD spectra of ΔE22-Aβ_{1-39} injected from neat HFIP into NaP [final HFIP concentration of 2% (v/v)] at 0 h, and 7 days later; Figure 7A shows spectra obtained under the same conditions for WT Aβ_{1-40}. The WT peptide spectrum was consistent with "random coil" at time zero but had converted to β-sheet by day 7, consistent with ThT and other data indicating conversion to a β-sheet fibril structure. In contrast, ΔE22-Aβ_{1-39} immediately exhibited a β-sheet CD spectrum, and this did not change after 7 days. To assess whether the peptide was in the fluid or solid phase, CD spectra of the peptide solution (or slurry) were recorded immediately after it had been dissolved and then after centrifugation at 14300g (top 1 mL of 1.5 mL in the centrifuge tube). As shown in Figure 7C, most of the signal for WT Aβ_{1-40} remained in the supernatant, while for ΔE22-Aβ_{1-39}, centrifugation caused a nearly total loss of signal, indicating that the β-sheet form of the peptide was insoluble and fibrillar, consistent with the electron microscopy data shown in Figure 2. [Similar experiments in which the peptides from DMSO were injected yielded similar results, but this solvent precludes measurements in the far-UV range (data not shown).] These results indicate that the preponderance of ΔE22-Aβ_{1-39} peptide giving a β-sheet was fibrillar, and not oligomers, which would have remained in the soluble phase.

Solid-State NMR Spectroscopy of ΔE22-Aβ_{1-39} Fibrils. Panels A and B of Figure 8 show PITHIRDS-CT data of two samples of ΔE22-Aβ_{1-39} fibrils, one containing a single 1-^{13}C label in V18 and the other with a single 1-^{13}C label in V36, respectively. For comparison, similar data are shown for WT Aβ_{1-40} fibrils containing a single 1-^{13}C label at V12 (Figure 8C). The decay of ^{13}C NMR signals (peak areas) with increasing dephasing time is related to the distance between ^{13}C labels, r, in adjacent peptide molecules, in a $1/r^3$ relationship. As described previously, in WT Aβ_{1-40} fibrils, which contain parallel, in-register β-sheets, this distance is ~5 ± 0.2 Å for V12, V18, and V36, indicating that these residues are within the parallel β-sheets.[7,8,38] This is not the case for the ΔE22-Aβ_{1-39} fibrils,

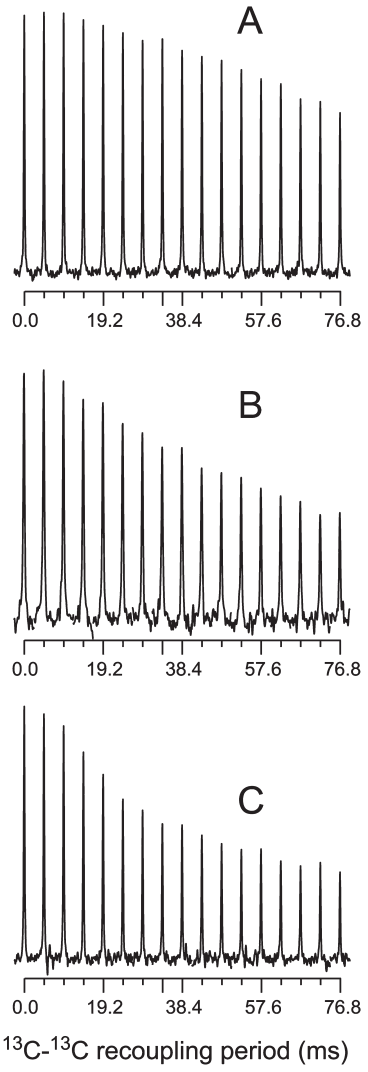

Figure 8. Raw PITHIRDS-CT data for rehydrated ΔE22-Aβ40 fibrils with 1-^{13}C labels at Val18 (A) and Val36 (B). For comparison, comparable data are provided for WT Aβ_{1-40} with a 1-^{13}C label at Val12 (C).

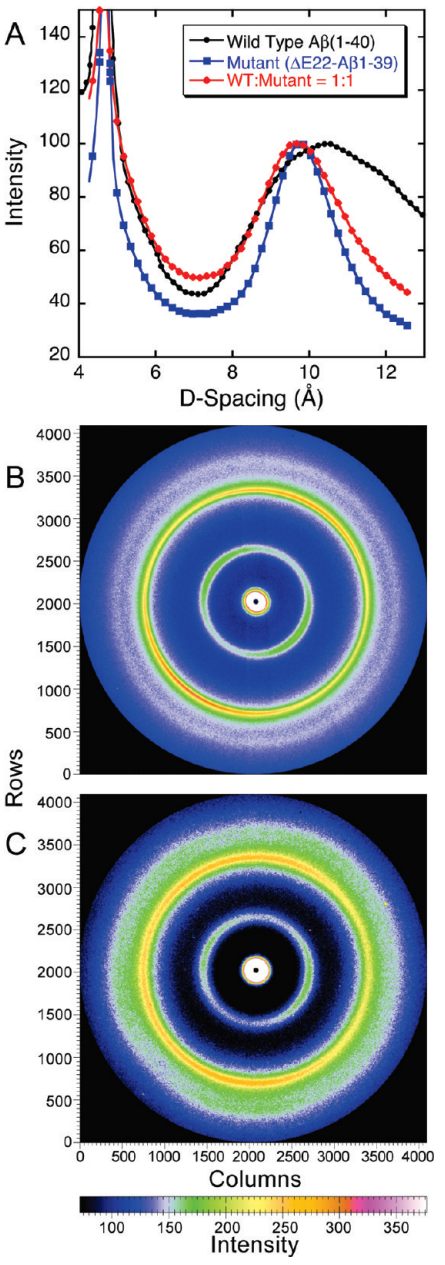

Figure 9. X-ray fiber diffraction pattern for partially aligned fibrils of ΔE22-Aβ_{1-39} and for fibrils formed from a 1:1 (molar) mixture of ΔE22-Aβ_{1-39} and WT Aβ_{1-40}. (A) One-dimensional azimuthal plots, showing intensity as a function of *D* spacing for WT Aβ_{1-40} (black), ΔE22-Aβ_{1-39} (red), and the 1:1 (molar) mixture of ΔE22-Aβ_{1-39} and WT Aβ_{1-40} (blue). The intensities have been normalized to the maximal intensity value of the peak of ∼10 Å spacing. The one-dimensional azimuthal plot for WT Aβ_{1-40} is from ref 19. (B) Pseudocolored plot of the X-ray diffraction pattern for ΔE22-Aβ_{1-39}. (C) Pseudocolored plot of the X-ray diffraction pattern for the 1:1 (molar) mixture of ΔE22-Aβ_{1-39} and WT Aβ_{1-40}.

which show a slower decay of the signal with increasing dephasing time, indicating that these residues are >6 Å apart and thus are not within parallel, in-register β-sheets.

X-ray Diffraction of ΔE22-Aβ_{1-39} Fibrils. Panel A of Figure 9 shows the one-dimensional azimuthal plots of partially aligned ΔE22-Aβ_{1-39} and WT Aβ_{1-40} fibrils. Panels B and C of Figure 9 show a pseudocolored plot of the diffraction data for ΔE22-Aβ_{1-39} fibrils and WT Aβ_{1-40} fibrils, respectively. A diffraction pattern most consistent with a "cross-β" structure is observed in both cases. The *D* spacings of the reflections differ between wild-type and mutant peptides, however. In both cases, a sharp, meridional reflection is observed at 4.7 Å. At right angles, there is a broad equatorial reflection, which is at 10.4 Å for WT Aβ_{1-40} but at 9.6 Å for ΔE22-Aβ_{1-39}. This latter value is quite similar to that observed for D23N-Aβ_{1-40}, which contained antiparallel β-sheet fibril structures.

"Prion-like" Behavior of ΔE22-Aβ_{1-39}. Most patients with the ΔE22 mutation of Aβ (i.e., the ΔE693 mutation of β-APP) are heterozygotes, and likely synthesize both ΔE22-Aβ_{1-39} and WT Aβ_{1-40}. Figure 1 shows the ThT fluorescence time course obtained when a 1:1 molar solution of ΔE22-Aβ_{1-39} and WT Aβ_{1-40} is mixed in neat DMSO (both at 50 μM, hence a total peptide concentration of 100 μM) and then diluted with aqueous buffer (NaP). The mixture forms fibrils very rapidly, though there is a brief buildup period in which ThT-associated fluorescence increases in the mixture (consistent with first-order

dx.doi.org/10.1021/bi1016217 |*Biochemistry* 2011, 50, 2026–2039

kinetics), which does not occur with pure ΔE22-Aβ_{1-39}. Thus, the presence of the WT peptide somewhat retards the fibrillization of ΔE22-Aβ_{1-39}. The final fluorescence value for the mixture obtained is identical to that obtained for pure ΔE22-Aβ_{1-39}, but notably, without a second phase that might be seen if the two peptides were fibrillizing in a manner independent of each other. If the WT peptide were not forming fibrils at all, one would expect the ThT fluorescence of a 1:1 mixture to be approximately half of that seen with 50 μM pure ΔE22-Aβ_{1-39}. Furthermore, if the wild-type and mutant peptides were fibrillizing in a manner independent of one another, the ThT fluorescence would be the average observed for the two different types of fibrils. The fact that the fluorescence of the mixed fibrils is identical to that of pure ΔE22-Aβ_{1-39} fibrils suggests that the rapidly fibrillizing mutant peptide forms a seed or template upon which the wild-type peptide deposits, also in a form that binds ThT poorly (using the assay of refs 19−23). As shown in panels G and H of Figure 2, electron microscopy shows that the mixture contained abundant fibrils, and no obvious amorphous precipitate, confirming that the WT peptide is also fibrillizing.

The kinetic pattern is consistent with rapid nucleation of ΔE22-Aβ_{1-39}, followed by accretion of WT Aβ_{1-40} onto nuclei or fibrils of the mutant peptide. If this is the case, then the mutant peptide would have "converted" the wild-type peptide to a structure of fibrils that it does not ordinarily adopt, i.e., other than a parallel in-register β-sheet. We performed an HPLC analysis of the supernatant remaining at various times during the fibrillization of the mixture, to determine the concentration of each peptide. As shown in Figure 3B of the Supporting Information, the concentration of soluble ΔE22-Aβ_{1-39} decayed more rapidly than that of WT Aβ_{1-40}, though not so rapidly as that of ΔE22-Aβ_{1-39} alone. The kinetics were consistent with first-order kinetics, with k values of 0.08 and 0.29 h^{-1} for WT Aβ_{1-40} and ΔE22-Aβ_{1-39}, respectively. Note that at the earliest measurable time point, more than half of the ΔE22-Aβ_{1-39} had already precipitated, whereas essentially all of the WT Aβ_{1-40} was still in solution. After fibrillization for 2 weeks, the supernatant contained 12.1 μM soluble ΔE22-Aβ_{1-39} and 32.6 μM WT Aβ_{1-40}. Both of these values are considerably higher than the critical concentrations, suggesting that the two peptides may be able to form a soluble mixed complex or several different types of complexes,
i.e., mixed dimers or oligomers.

To test the hypothesis further that ΔE22-Aβ_{1-39} had converted WT Aβ_{1-40} to an alternate structure, we performed X-ray diffraction of the mixed fibrils. As shown in Figure 9C, the mixed fibrils also showed a cross-β pattern, but with D spacings essentially identical to those of the pure ΔE22-Aβ_{1-39} fibrils, and clearly distinct from those of WT Aβ_{1-40} fibrils, i.e., a sharp, meridional reflection at 4.7 Å and a broad equatorial reflection, which is at 9.6 Å. In other words, the D spacings were those of the more rapidly fibrillizing species and were not means of the two sets of values. These results agree with the ThT fluorescence results in suggesting that the rapidly fibrillizing ΔE22-Aβ_{1-39} fibrils served as a seed or template for the WT peptide, "converting" the latter to some structure other than the usual parallel, in-register β-sheet.

DISCUSSION

Contrary to previous reports,[11,17,39] ΔE22-Aβ_{1-39} forms amyloid fibrils extremely rapidly and with essentially complete conversion of the soluble peptide to fibrils. The fibrils have most of the hallmarks of amyloid, such as β-sheet structure as determined by CD spectroscopy and X-ray diffraction, Congo Red binding, and electron microscopic appearance, though a slight difference exists in mean fibril diameter between WT Aβ_{1-40} and ΔE22-Aβ_{1-39} fibrils. Formation of fibrils and adoption of β-sheet structure are virtually instantaneous, as shown by ThT fluorescence, electron microscopy, CD spectroscopy, and fluorescence depolarization. Size exclusion chromatography indicates that ΔE22-Aβ_{1-39} can form oligomers under some conditions [e.g., when 2% (v/v) DMSO is present in the eluant], but these are short-lived and very rapidly progress toward fibril formation. The critical concentration of ΔE22-Aβ_{1-39} was ∼1 order of magnitude lower than that of WT-Aβ_{1-40} (2.89 and 0.167 μM for WT Aβ_{1-40} and ΔE22-Aβ_{1-39}, respectively). The value we obtained for the WT peptide was slightly higher than that obtained by O'Nuallain et al.,[28] presumably because of small differences in methodology. Nonetheless, our data suggest a substantial difference in the intrinsic solubilities of the two peptides.

One notable exception to the statement that ΔE22-Aβ_{1-39} forms typical amyloid fibrils is that the fibrils are associated with little ThT fluorescence, suggesting structural differences between these fibrils and those made by the WT peptide. We also showed that ΔE22-Aβ_{1-39} fibrils do bind ThT, though with a lower affinity, and with fewer apparent binding sites per mass of peptide. At least two explanations for this difference suggest themselves. First, electron microscopy of ΔE22-Aβ_{1-39} shows the presence of matted and supertwisted fibrils; these supramolecular structural features may block access of ThT to potential binding sites. When ThT is included in the solution in which fibrils are forming, a large difference between the ThT fluorescence of WT and mutant Aβ remains, suggesting that the difference is due to structural differences, as well as decreased access of matted fibrils for the dye. Second, recent studies,[25−27] from both experimental data and molecular dynamics simulations of the binding of ThT and other dyes to Aβ fragments, suggest that ThT binding and fluorescence require an aromatic−hydrophobic groove spanning four consecutive β-strands. Distortion of this groove in the mutant peptide fibrils might allow some ThT binding, albeit at somewhat lower affinity, but abrogate the associated fluorescence. Thus, differences in ThT binding suggest structural differences between WT Aβ_{1-40} and ΔE22-Aβ_{1-39} fibrils. Other clear indications of structural differences between these types of fibrils came from solid-state NMR measurements and the X-ray diffraction patterns of ΔE22-Aβ_{1-39} fibrils. In PITHIRDS-CT spectra, the distance between degenerate ^{13}C spins in adjacent molecules of WT Aβ_{1-40} fibrils is ∼5.0 ± 0.2 Å, consistent with a parallel, in-register β-strand structure. In contrast, at two sites of ΔE22-Aβ_{1-39}, (1-^{13}C-V18 and 1-^{13}C-V36), the PITHIRDS-CT spectra were inconsistent with this structure. X-ray diffraction showed a clear difference between the WT and mutant peptide fibrils: the broad equatorial reflections were at 10.4 and 9.6 Å for WT Aβ_{1-40} and ΔE22-Aβ_{1-39}, respectively. Further solid-state NMR work to delineate the structural features of these fibrils is ongoing.

Most patients with the ΔE693-Aβ-APP mutation are heterozygotes and thus, presumably, synthesize both wild-type and mutant forms of Aβ. Recent studies of another point mutant of the Aβ peptide, D23N-Aβ_{1-40}, suggest that even fairly subtle sequence changes can lead to drastic change in fibril structure:[21] the latter mutant forms fibrils with antiparallel β-sheet structure,

in contrast to all previous observed structures of full-length Aβ. Here, we show that when a 1:1 solution of WT $A\beta_{1-40}$ and ΔE22-$A\beta_{1-39}$ was mixed in neat DMSO prior to fibrillization, the fibrils formed by this mixture had ThT fluorescence levels essentially identical to that of the mutant peptide fibrils alone. Both of the peptides were within the fibrils; a sedimentation assay of these mixtures showed that both peptides had precipitated, and electron microscopy showed fibrils and no amorphous precipitate, indicating that both peptides had formed fibrils. Furthermore, the electron microscopic appearance of the mixed fibrils was quite similar to that of the pure ΔE22-$A\beta_{1-39}$ fibrils, i.e., matted and supertwisted bundles of slightly irregular fibrils. Finally, and most convincingly, X-ray diffraction of the mixed fibrils showed a pattern essentially identical to that of the pure ΔE22-$A\beta_{1-39}$ fibrils and distinct from that of the WT $A\beta_{1-40}$ fibrils, and, furthermore, not a mean of the two sets of values. Taken together, these results suggest that the rapidly aggregating ΔE22-$A\beta_{1-39}$ peptide formed fibril seeds, which WT $A\beta_{1-40}$ extended, with a structure resembling that of the mutant fibrils rather than that of typical WT $A\beta_{1-40}$ fibrils. This type of "conversion" of the wild-type peptide into an atypical structure is reminiscent of the conversion of prion species, which has been observed in vitro for both yeast[40−42] and mammalian[43−45] prion proteins, as well as for amyloids of β2-microglobulin.[46,47] By the same token, another rapidly fibrillizing point mutant form of Aβ, E22Q-Aβ (the Dutch mutant), has been shown to cross-seed fibril extension by the wild-type peptide.[48]

Finally, these studies may have implications for the pathogenesis of early onset AD in this kindred. Two likely explanations for the negative Pittsburgh B brain scan cannot be distinguished at present. These are a lack of ΔE22-$A\beta_{1-39}$ amyloid deposition in the brains of these patients and, alternatively, a lack of binding by Pittsburgh B, which is structurally homologous to ThT. The rapidity with which ΔE22-$A\beta_{1-39}$ forms fibrils, however, suggests that extensive protein aggregation could occur within neurons, even leading to intracellular formation of fibrils. Indeed, Tomiyama et al. have documented a very low level of Aβ secretion by cells transfected with the ΔE693 mutant form of β-APP. The sparseness and transience of soluble oligomers of ΔE22-$A\beta_{1-39}$ also suggest that soluble oligomeric species may not be necessary for neuronal death in all forms of Alzheimer's disease. Recently, a transgenic mouse model of the ΔE693-Aβ-APP mutation has been described.[49] These mice exhibited age-dependent accumulation of intraneuronal Aβ, which coincided with the development of neuronal degeneration and glial cell reaction. The observation that no neuritic plaques developed should not, however, be construed to mean that only oligomers are present; fibrils developing within neurons could easily escape detection, and "fibrils" should never be equated with "plaques". This study underscores the complexity of the pathogenesis of this disease and indicates that multiple pathogenic mechanisms may be at play.

■ ASSOCIATED CONTENT

Supporting Information. Sample chromatograph for the RP-HPLC assay of thioflavin T concentration, calibration curve for the RP-HPLC assay of thioflavin T concentration, calibration curves for the mass of WT $A\beta_{1-40}$ and ΔE22-$A\beta_{1-39}$, sample chromatograph for the separation and quantitation of ΔE22-$A\beta_{1-39}$ and WT $A\beta_{1-40}$ in mixtures, and HPLC analysis of concentrations of ΔE22-$A\beta_{1-39}$ and WT $A\beta_{1-40}$ remaining in solution, in fibrillizing mixtures of the two peptides. This material is available free of charge via the Internet at http://pubs.acs.org.

■ AUTHOR INFORMATION

Corresponding Author

*Department of Pathology, The University of Chicago, 5841 S. Maryland Ave., Chicago, IL 60637. Phone: (773) 702-1267. Fax: (773) 834-5251. E-mail: scmeredi@uchicago.edu.

Notes

[a]This term refers to the analogue of WT $A\beta_{1-40}$. Although it is sometimes termed ΔE22-$A\beta_{1-40}$, it has only 39 amino acids, and therefore, we prefer to call it ΔE22-$A\beta_{1-39}$. This sequence of this peptide is given in the Materials and Methods.

Funding Sources

We acknowledge support from the National Institutes of Health (NIH) (Grant NS042852 to S.C.M.), the Alzheimer's Association (Grant IIRG-06-27794 to S.C.M.), and the National Science Foundation (MCB-0644015 CAREER, J.P.R.O.O.). This work was supported in part by the Intramural Research Program of the National Institute of Diabetes and Digestive and Kidney Diseases of the National Institutes of Health. Use of the Advanced Photon Source was supported by the U.S. Department of Energy, Basic Energy Sciences, Office of Science, under Contract W-31-109-ENG-38. BioCAT is a National Institutes of Health-supported Research Center (Grant RR-08630).

■ ABBREVIATIONS

Aβ, β-amyloid; MW^{app}, apparent molecular weight; β-APP, β-amyloid precursor protein; CD, circular dichroism; C_r, critical concentration; DMSO, dimethyl sulfoxide; HFIP, hexafluoro-2-propanol; HPLC, high-performance liquid chromatography; HBTU, 2-(1*H*-benzotriazol-1-yl)-1,1,3,3-tetramethyluronium hexafluorophosphate; HOBT, *N*-hydroxybenzotriazole; MALDI-TOF, matrix-assisted laser desorption ionization time-of-flight; MAS, magic angle spinning; NaP, 10 mM sodium phosphate (pH 7.40) with 0.01% NaN_3; Rf, radiofrequency; RP, reverse phase; SEC, size exclusion chromatography; SS-NMR, solid-state nuclear magnetic resonance; TFA, trifluoroacetic acid; ThT, thioflavin T; WT, wild-type.

■ REFERENCES

(1) Levy, E., Carman, M. D., Fernandez-Madrid, I. J., Power, M. D., Lieberburg, I., van Duinen, S. G., Bots, G. T. A. M., Luyendijk, W., and Frangione, B. (1990) Mutation of the Alzheimer's disease amyloid gene in hereditary cerebral hemorrhage, Dutch type. *Science 248*, 1124–1126.

(2) Van Broeckhoven, C., Haan, J., Bakker, E., Hardy, J. A., Van Hul, W., Wehnert, A, Vegter-Van der Vlis, M., and Roos, R. A. C. (1990) Amyloid β protein precursor gene and hereditary cerebral hemorrhage with amyloidosis (Dutch). *Science 248*, 1120–1122.

(3) Cras, P., van Harskamp, F., Hendriks, L., Ceuterick, C., van Duijn, C. M., Stefanko, S. Z., Hofman, A., Kros, J. M., Van Broeckhoven, C., and Martin, J. J. (1998) Presenile Alzheimer dementia characterized by amyloid angiopathy and large amyloid core type senile plaques in the APP 692Ala → Gly mutation. *Acta Neuropathol. 96*, 253–260.

(4) Tagliavini, F., Rossi, G., Padovani, A., Magoni, M., Andora, G., Sgarzi, M., Bizzi, A., Savioardo, M., Carella, F., Morbin, M., Giaccone, G., and Bugiani, O. (1999) A new bPP mutation related to hereditary cerebral haemorrhage. *Alzheimer's Rep. 2* (Suppl.), S28.

(5) Nilsberth, C., Westlind-Danielsson, A., Eckman, C. B., Condron, M. M., Axelman, K., Forsell, C., Stenh, C., Luthman, J., Teplow, D. B.,

Younkin, S. G., Näslund, J., and Lannfelt, L. (2001) The 'Arctic' APP mutation (E693G) causes Alzheimer's disease by enhanced Aβ protofibril formation. *Nat. Neurosci. 4*, 887–893.

(6) Grabowski, T. J., Cho, H. S., Vonsattel, J. P., Rebeck, G. W., and Greenberg, S. M. (2001) Novel amyloid precursor protein mutation in an Iowa family with dementia and severe cerebral amyloid angiopathy. *Ann. Neurol. 49*, 697–705.

(7) Petkova, A. T., Ishii, Y., Balbach, J. J., Antzutkin, O. N., Leapman, R. D., Delaglio, F., and Tycko, R. (2002) A structural model for Alzheimer's β-amyloid fibrils based on experimental constraints from solid state NMR. *Proc. Natl. Acad. Sci. U.S.A. 99*, 16742–16747.

(8) Balbach, J. J., Petkova, A. T., Oyler, N. A., Antzutkin, O. N., Gordon, D. J., Meredith, S. C., and Tycko, R. (2002) Supramolecular structure in full-length Alzheimer's β-amyloid fibrils: Evidence for a parallel β-sheet organization from solid-state nuclear magnetic resonance. *Biophys. J. 83*, 1205–1216.

(9) Paravastu, A. K., Leapman, R. D., Yau, W. M., and Tycko, R. (2008) Molecular structural basis for polymorphism in Alzheimer's β-amyloid fibrils. *Proc. Natl. Acad. Sci. U.S.A. 105*, 18349–18354.

(10) Tycko, R. (2006) Molecular structure of amyloid fibrils: Insights from solid-state NMR. *Q. Rev. Biophys. 39*, 1–55.

(11) Tomiyama, T., Nagata, T., Shimada, H., Teraoka, R., Fukushima, A., Kanemitsu, H., Takuma, H., Kuwano, R., Imagawa, M., Ataka, S., Wada, Y., Yoshioka, E., Nishizaki, T., Watanabe, Y., and Mori, H. (2008) A new amyloid β variant favoring oligomerization in Alzheimer's-type dementia. *Ann. Neurol. 63*, 377–387.

(12) Hardy, J. A., and Higgins, G. A. (1992) Alzheimer's disease: The amyloid cascade hypothesis. *Science 256*, 184–185.

(13) Tanzi, R. E., and Bertram, L. (2005) Twenty years of the Alzheimer's disease amyloid hypothesis: A genetic perspective. *Cell 120*, 545–555.

(14) Klein, W. L., Stine, W. B., Jr., and Teplow, D. B. (2004) Small assemblies of unmodified amyloid β-protein are the proximate neurotoxin in Alzheimer's disease. *Neurobiol. Aging 25*, 569–580.

(15) Bitan, G., Fradinger, E. A., Spring, S. M., and Teplow, D. B. (2005) Neurotoxic protein oligomers: What you see is not always what you get. *Amyloid 12*, 88–95.

(16) Lesné, S., Koh, M. T., Kotilinek, L., Kayed, R., Glabe, C. G., Yang, A., Gallagher, M., and Ashe, K. H. (2006) A specific amyloid-β protein assembly in the brain impairs memory. *Nature 440*, 352–357.

(17) Nishitsuji, K., Tomiyama, T., Ishibashi, K., Ito, K., Teraoka, R., Lambert, M. P., Klein, W. L., and Mori, H. (2009) The E693Δ mutation in amyloid precursor protein increases intracellular accumulation of amyloid β oligomers and causes endoplasmic reticulum stress-induced apoptosis in cultured cells. *Am. J. Pathol. 174*, 957–969.

(18) Klunk, W. E., Pettegrew, J. W., and Abraham, D. J. (1989) Quantitative evaluation of congo red binding to amyloid-like proteins with a β-pleated sheet conformation. *J. Histochem. Cytochem. 37*, 1273–1282.

(19) Naiki, H., Higuchi, K., Hosokawa, M., and Takeda, T. (1989) Fluorometric determination of amyloid fibrils in vitro using the fluorescent dye, thioflavin T1. *Anal. Biochem. 177*, 244–249.

(20) Sciarretta, K. L., Gordon, D. J., Petkova, A. T., Tycko, R., and Meredith, S. C. (2005) Aβ40-Lactam(D23/K28) Models a Conformation Highly Favorable for Nucleation of Amyloid. *Biochemistry 44*, 6003–6014.

(21) Tycko, R., Sciarretta, K. L., Orgel, P. R. O., and Meredith, S. C. (2009) Evidence for Novel β-Sheet Structures in Iowa Mutant β-Amyloid Fibrils. *Biochemistry 48*, 6072–6084.

(22) LeVine, H., III (1999) Quantification of β-sheet amyloid fibril structures with thioflavin T. *Methods Enzymol. 309*, 274–284.

(23) LeVine, H., III (1993) Thioflavine T interaction with synthetic Alzheimer's disease β-amyloid peptides: Detection of amyloid aggregation in solution. *Protein Sci. 2*, 404–410.

(24) Finder, W. H., Vodopivec, I., Nitsch, R. M., and Rudi Glockshuber, R. (2010) The recombinant amyloid-β peptide Aβ1−42 aggregates faster and is more neurotoxic than synthetic Aβ1−42. *J. Mol. Biol. 396*, 9–18.

(25) Biancalana, M., Makabe, K., Koide, A., and Koide, S. (2009) Molecular mechanism of thioflavin-T binding to the surface of β-rich peptide self-assemblies. *J. Mol. Biol. 385*, 1052–1063.

(26) Wu, C., Biancalana, M., Koide, S., and Shea, J. E. (2009) Binding modes of thioflavin-T to the single-layer β-sheet of the peptide self-assembly mimics. *J. Mol. Biol. 394*, 627–633.

(27) Biancalana, M., and Koide, S. (2010) Molecular mechanism of Thioflavin-T binding to amyloid fibrils. *Biochim. Biophys. Acta 1804*, 1405–1412.

(28) O'Nuallain, B., Shivaprasad, S., Kheterpal, I., and Wetzel, R. (2005) Thermodynamics of Aβ(1−40) Amyloid Fibril Elongation. *Biochemistry 44*, 12709–12718.

(29) Lanning, J. D., Hawk, A. J., Derryberry, J., and Meredith, S. C. (2010) Chaperone-like *N*-methyl Peptide Inhibitors of Polyglutamine Aggregation. *Biochemistry 49*, 7108–7118.

(30) Stubbs, G. (1999) Developments in fiber diffraction. *Curr. Opin. Struct. Biol. 9*, 615–619.

(31) Torbet, J. (1987) Using magnetic orientation to study structure and assembly. *Trends Biochem. Sci. 12*, 327–330.

(32) Lakowicz, J. R. (1983) *Principles of Fluorescence Spectroscopy*, Chapter 5, Plenum Press, New York.

(33) Tycko, R. (2007) Symmetry-based constant-time homonuclear dipolar recoupling in solid state NMR. *J. Chem. Phys. 126*, 064506.

(34) Zhang, O., Kay, L. E., Olivier, J. P., and Forman-Kay, J. D. (1994) Backbone ^{1}H and ^{15}N resonance assignments of the N-terminal SH3 domain of drk in folded and unfolded states using enhanced-sensitivity pulsed field gradient NMR techniques. *J. Biomol. NMR 4*, 845–858.

(35) Jarrett, J. T., and Lansbury, P. T., Jr. (1993) Seeding "One-Dimensional Crystallization" of Amyloid: A Pathogenic Mechanism in Alzheimer's Disease and Scrapie? *Cell 73*, 1055–1059.

(36) Thirumalai, D., Klimov, D. K., and Dima, R. I. (2003) Emerging ideas on the molecular basis of protein and peptide aggregation. *Curr. Opin. Struct. Biol. 13*, 146–159.

(37) Kodaka, M. (2004) Requirements for generating sigmoidal time-course aggregation in nucleation-dependent polymerization model. *Biophys. Chem. 107*, 243–253.

(38) Petkova, A. T., Yau, W.-M., and Tycko, R. (2006) Experimental Constraints on Quaternary Structure in Alzheimer's β-Amyloid Fibrils. *Biochemistry 45*, 498–512.

(39) Takuma, H., Teraoka, R., Mori, H., and Tomiyama, T. (2008) Amyloid β E22Δ variant induces synapse alteration in mouse hippocampal slices. *NeuroReport 19*, 615–619.

(40) DePace, A. H., and Weissman, J. S. (2002) Origins and kinetic consequences of diversity in Sup35 yeast prion fibers. *Nat. Struct. Biol. 9*, 389–396.

(41) Vitrenko, Y. A., Gracheva, E. O., Richmond, J. E., and Liebman, S. W. (2007) Visualization of aggregation of the Rnq1 prion domain and cross-seeding interactions with Sup35NM. *J. Biol. Chem. 282*, 1779–1787.

(42) Toyama, B. H., Kelly, M. J., Gross, J. D., and Weissman, J. S. (2007) The structural basis of yeast prion strain variants. *Nature 449*, 233–237.

(43) Makarava, N., Ostapchenko, V. G., Savtchenko, R., and Baskakov, I. V. (2009) Conformational switching within individual amyloid fibrils. *J. Biol. Chem. 284*, 14386–14395.

(44) Kodali, R., and Wetzel, R. (2007) Polymorphism in the intermediates and products of amyloid assembly. *Curr. Opin. Struct. Biol. 17*, 48–57.

(45) Cobb, N. J., and Surewicz, W. K. (2009) Prion diseases and their biochemical mechanisms. *Biochemistry 48*, 2574–2585.

(46) Yamaguchi, K., Takahashi, S., Kawai, T., Naiki, H., and Goto, Y. (2005) Seeding-dependent propagation and maturation of amyloid fibril conformation. *J. Mol. Biol. 352*, 952–960.

(47) Kihara, M., Chatani, E., Sakai, M., Hasegawa, K., Naiki, H., and Goto, Y. (2005) Seeding-dependent maturation of β2-microglobulin amyloid fibrils at neutral pH. *J. Biol. Chem. 280*, 12012–12018.

(48) Miravalle, L., Tokuda, T., Chiarle, R., Giaccone, G., Bugiani, O., Tagliavini, F., Frangione, B., and Ghiso, J. (2000) Substitutions at codon 22 of Alzheimer's Aβ peptide induce diverse conformational changes and apoptotic effects in human cerebral endothelial cells. *J. Biol. Chem. 275*, 27110–27116.

(49) Tomiyama, T., Matsuyama, S., Iso, H., Umeda, T., Takuma, H., Ohnishi, K., Ishibashi, K., Teraoka, R., Sakama, N., Yamashita, T., Nishitsuji, K., Ito, K., Shimada, H., Lambert, M. P., Klein, W. L., and Mori, H. (2010) A Mouse Model of Amyloid β Oligomers: Their Contribution to Synaptic Alteration, Abnormal Tau Phosphorylation, Glial Activation, and Neuronal Loss In Vivo. *J. Neurosci. 30*, 4845–4856.